Original Article

AI-assisted compressed sensing MRI improves imaging quality in rectal cancer: a comparative study with conventional acceleration techniques

Guangying Zheng[1,2], Junyi Fu[1], Zhe Wang[1], Wei Li[1]^, Aiyin Li[1], Dan Yu[3]

[1]Department of Radiology, The First Affiliated Hospital of Shandong First Medical University & Shandong Provincial Qianfoshan Hospital, Shandong Lung Cancer Institute, Shandong Institute of Neuroimmunology, Jinan, China; [2]Department of Graduate, Shandong First Medical University and Shandong Academy of Medical Sciences, Jinan, China; [3]United Imaging Research Institute of Intelligent Imaging, Beijing, China

Contributions: (I) Conception and design: W Li, A Li; (II) Administrative support: A Li; (III) Provision of study materials or patients: D Yu, Z Wang; (IV) Collection and assembly of data: G Zheng, J Fu; (V) Data analysis and interpretation: G Zheng; (VI) Manuscript writing: All authors; (VII) Final approval of manuscript: All authors.

Correspondence to: Wei Li, MD; Aiyin Li, MD. Department of Radiology, The First Affiliated Hospital of Shandong First Medical University & Shandong Provincial Qianfoshan Hospital, Shandong Lung Cancer Institute, Shandong Institute of Neuroimmunology, 16766 Jingshi Road, Jinan 250014, China. Email: lwqfsh@126.com; 13953101875@139.com.

Background: Artificial intelligence (AI)-assisted compressed sensing (ACS) is widely used in various parts of the body, but the application of this technology in the rectum is still rare. This study aimed to evaluate the feasibility of super-resolution (SR) T2-weighted imaging (T2WI) based on ACS in rectal cancer (RC) by comparing with compressed sensing (CS) and parallel imaging (PI).

Methods: In this prospective study, 29 patients with rectal adenocarcinoma were enrolled, and three groups of SR rectal T2WI images based on ACS, CS, and PI (ACS-T2WI, CS-T2WI, and PI-T2WI) were obtained, using the same scanning time for each group. Two radiologists independently assessed the visibility of structures, tissue edge sharpness, image artifacts, overall image quality, and confidence in N staging for the three sequences using a five-point Likert scale; the scores of the three sequences were compared and the agreement between two readers was assessed. In addition, the quantitative parameters of the three groups, sharpness, signal-to-noise ratio (SNR), and contrast-to-noise ratio (CNR) were compared. T staging based on magnetic resonance imaging (MRI) was performed by two readers separately using the three sequences combined with other conventional scanning sequences. The consistency between T staging based on MRI (mrT staging) and pathological T staging (PT staging) of the two readers and the diagnostic accuracy of every sequence was compared.

Results: The scores of ACS-T2WI were higher in visibility of structures, tissue edge sharpness, overall image quality, and confidence in N staging than CS-T2WI and PI-T2WI ($P<0.001$). There was no statistical difference in the scores of image artifacts among the three sequences ($P=0.18$). The sharpness of ACS-T2WI was higher than that of CS-T2WI and PI-T2WI ($P<0.001$). The SNR of CS-T2WI was slightly higher than that of ACS-T2WI and PI-T2WI ($P=0.004$). There was no statistically significant difference in CNR among the three sequences ($P=0.425$). The consistency between mrT staging of ACS-T2WI and PT staging was higher than that of CS-T2WI and PI-T2WI. The two readers had a higher diagnostic accuracy for ACS-T2WI (89.66%) than for CS-T2WI (79.31%) and PI-T2WI (75.86%), but the difference was not statistically significant.

Conclusions: By using ACS to increase the resolution through a larger matrix size, higher quality images can be obtained within the same scanning time as traditional acceleration techniques. The SR T2WI based

^ ORCID: 0000-0002-4758-2883.

on ACS can be well applied in the clinical scanning of RC.

Keywords: Rectal cancer (RC); magnetic resonance imaging (MRI); artificial intelligence (AI); super resolution

Submitted Jun 28, 2024. Accepted for publication Nov 11, 2024. Published online Dec 28, 2024.
doi: 10.21037/qims-24-1317
View this article at: https://dx.doi.org/10.21037/qims-24-1317

Introduction

Colorectal cancer is one of the most common digestive tumors and the leading cause of cancer mortality worldwide, with rectal cancer (RC) accounting for one-third of these cases (1). Timely screening, diagnosis, and treatment measures can effectively reduce its morbidity and mortality and improve the quality of life of patients (2). The appropriate treatment plan for RC depends on the tumor-node-metastasis (TNM) staging system, extramural venous invasion (EMVI), and mesorectal fascia (MRF) involvement (3,4). Magnetic resonance imaging (MRI) has the advantages of good tissue resolution, no ionizing radiation and non-invasiveness, and can provide high-resolution images, especially high-resolution T2-weighted imaging (T2WI), which is crucial for showing the details of tumor, lymph nodes, EMVI, and MRF (3,5,6). Therefore, it is the first choice for T and N staging, EMVI, and MRF of RC.

MRI acquisition is limited by long duration and related artifacts, which require high tolerance and compliance from patients. Currently, some acceleration methods by K-space undersampling such as partial Fourier (PF), parallel imaging (PI), and compressed sensing (CS) have been widely used in MRI acquisition to accelerate the scanning process to the duration that patients can tolerate (7). However, if the acceleration factor of these acceleration techniques is too large, noise, aliasing artifacts, and signal degradation will be unavoidable, resulting in the degradation of image quality and the reduced visibility of rectal wall, small lymph nodes, and vessels, which will affect the accuracy of T and N staging of RC patients (8,9). Therefore, improving the spatial resolution of the image at the appropriate scanning time to increase the visibility of the above structures is vital for the diagnosis and staging of RC.

As a branch of artificial intelligence (AI), deep learning (DL) has been widely used in the diagnosis and treatment of RC, but its application in the process of RC MRI acquisition is not common (10-16). The most commonly used neural network in medical imaging, the convolutional neural network (CNN), plays a key role in accelerating imaging by detecting more complex feature levels (17). Although CNN-based methods demonstrate exceptional reconstruction quality, their application in clinical environments is often hindered by unpredictability, attributed to the networks' opaque, "black-box" nature. The AI-assisted compressed sensing (ACS) used in this study effectively mitigates this uncertainty by incorporating the output from the AI module as a supplementary constraint within the CS framework. This is achieved through the introduction of a regularization term that addresses the divergence between images reconstructed via traditional methods and those predicted by AI (18).

ACS developed by United Imaging (Shanghai, China) is a technology that introduces a DL algorithm combined with conventional acceleration techniques such as PI and CS into an MRI reconstruction algorithm. Previous studies have shown that this kind of technology can effectively shorten the scanning time and suppress noise, and it has been widely used in the lumbar spine, breast, joint, abdomen, heart, and other areas (7,8,19-22). However, there have been few studies about this technique in RC. This study aimed to evaluate the image quality and diagnostic performance of super-resolution (SR) T2WI based on the ACS, which enables the use of a larger acquisition matrix within the same scanning time, compared to CS and PI. We present this article in accordance with the GRRAS reporting checklist (available at https://qims.amegroups.com/article/view/10.21037/qims-24-1317/rc).

Methods

Patients

This study was approved by Medical Ethics Committee of The First Affiliated Hospital of Shandong First Medical University (No. YXLL-KY-073). The study was conducted in accordance with the ethical standards of the Declaration of Helsinki (as revised in 2013) and all participants from The First Affiliated Hospital of Shandong First Medical University in this study signed written informed consent.

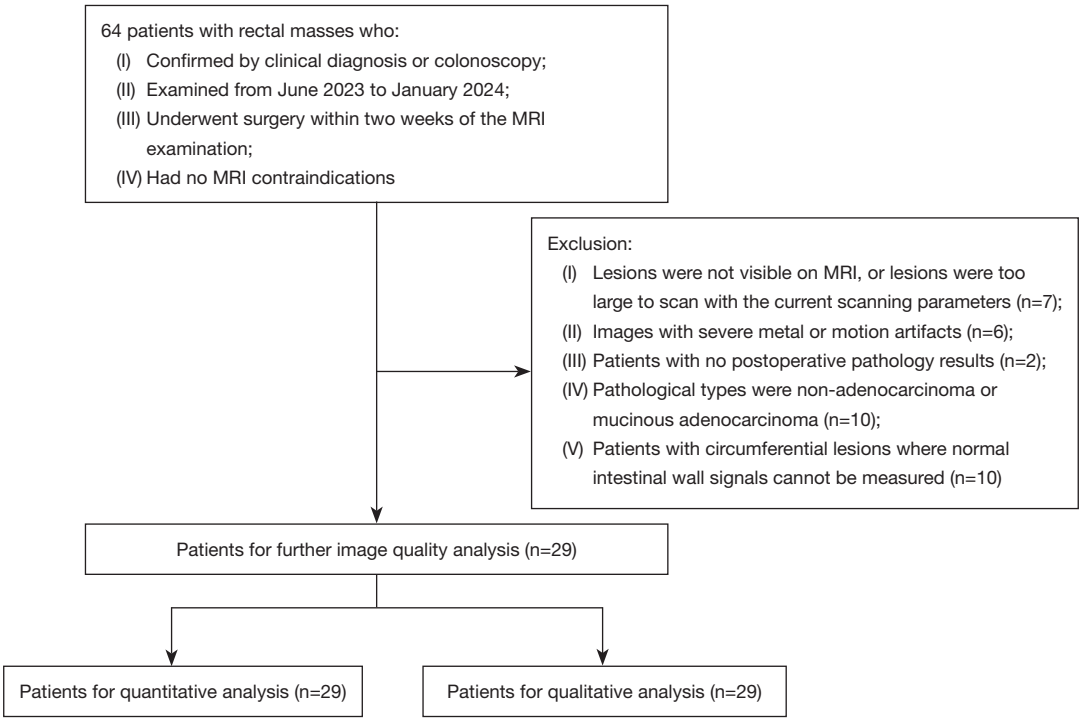

Figure 1 Flowchart of the enrolled patients. MRI, magnetic resonance imaging.

Initially, 64 patients with suspected RC were prospectively and continuously enrolled from June 2023 to January 2024. The inclusion criteria were as follows: (I) patients had rectal masses confirmed either clinically or by colonoscopy; (II) patients were diagnosed for the first time and did not receive any treatment (neoadjuvant treatment and surgery); (III) patients underwent surgery within two weeks of the MRI examination; and (IV) patients had no MRI contraindications. The exclusion criteria were as follows: (I) lesions were not visible on MRI, or lesions were too large to scan with the current scanning parameters; (II) severe image artifacts; (III) without postoperative pathological staging results; (IV) pathological types were non-adenocarcinoma or mucinous adenocarcinoma; and (V) patients with circumferential lesions where normal intestinal wall signals cannot be measured. Finally, 29 patients were included; the flowchart for the enrolment process is shown in *Figure 1*.

MRI acquisition

All MRI examinations were performed on a 3 T magnetic resonance (MR) scanner, using a 12-channel phased-array body coil (uMR790; United Imaging Healthcare, Shanghai, China), with the patient in the supine position. A glycerin enema was administered 2 hours before the examination to clean the intestinal tract. At 30 minutes before the MRI scan, 10 mg of anisodamine was injected to reduce intestinal peristalsis. Before the MRI scan, the patient's rectal lumen was filled with ultrasound transmission gel (60–100 mL, determined by lesion location, ultrasonic coupling agent mixed with water at 1:1), and the abdomen was pressurized with a sandbag to reduce respiratory movement artifacts. The MRI protocol included sagittal T2WI, coronal T2WI, axial T2WI, axial T1-weighted imaging (T1WI), axial diffusion-weighted imaging (DWI), and three oblique axial SR T2WI which are based on interpolation technology. The main imaging sequences and parameters of the MRI protocol are listed in *Table 1*.

Image analysis

Qualitative image analysis

All image post-processing was performed on an uWS-MrR005 workstation (United Imaging). The images were independently evaluated by two radiologists (reader 1, reader 2) with 16 years and 2 years of experience in abdominal imaging diagnosis, respectively, who were blinded to patient information and the specific imaging

Table 1 Main imaging sequences and parameters

Sequence	TR (ms)	TE (ms)	Thickness/ gap (mm)	Matrix	Reconstruction matrix	Number of echoes	FOV	Acceleration factor	Acquisition time(s)	NEX	Bandwidth (HZ/pixel)
ACS-T2WI	2,464	98.44	3.0/0.3	352×352	704×704	23	180×180	4	168	3.7	270
CS-T2WI	2,400	98.12	3.0/0.3	256×256	512×512	23	180×180	2	168	2.4	270
PI-T2WI	2,400	98.12	3.0/0.3	256×256	512×512	23	180×180	1.79	168	2.4	270

TR, repetition time; TE, echo time; FOV, field of view; NEX, number of excitations; ACS, artificial intelligence-assisted compressed sensing; CS, compressed sensing; PI, parallel imaging; T2WI, T2-weighted imaging; ACS-T2WI, T2WI images based on ACS; CS-T2WI, T2WI images based on CS; PI-T2WI, T2WI images based on PI.

sequence data to ensure unbiased analysis. The two readers analyzed images from ACS-T2WI, CS-T2WI, and PI-T2WI by using a five-point Likert scale, including visibility of structures, tissue edge sharpness, image artifacts, overall image quality, and confidence in N staging; the results of each sequence score were expressed as the average of two readers. The scale criteria were as follows (23-25):

(I) Visibility of structures (rectum, lymph nodes, tumor, vasculature): 0: completely invisible; 1: visible but very faint; 2: visible and slightly blurred; 3: visible and barely blurred; and 4: clearly visible.
(II) Tissue edges sharpness (stratification of rectal wall, margin of lesion): 0: completely invisible; 1: blurry and difficult to identify; 2: blurry but identifiable; 3: barely blurry and identifiable; and 4: clear and sharp.
(III) Image artifacts: 0: many but still diagnosable; 1: moderate; 2: few, 3: almost non-existent; 4: absent.
(IV) Overall image quality: 0: very poor; 1: poor, 2: fair; 3: good; and 4: excellent.
(V) Confidence in N staging: 0: non-diagnostic; 1: difficult to diagnose; 2: barely diagnosable; 3: diagnosable; and 4: easily diagnosable.

Quantitative image analysis

The image sharpness method proposed by Xin *et al.* (26) was used to calculate the sharpness of each group of images though the use of MATLAB 2016b (MathWorks, Natick, MA, USA). The range of sharpness is 0–1, with higher sharpness values indicating clearer images, and vice versa, more blurred images. The regions of interest on the lesion (ROI_{lesion}, about 5 mm^2) were delineated at layers where lesions and normal bowel walls coexisted on the three groups of images; the same location and size on three sets of images and three consecutive layers were outlined for each patient. The signal intensity of the ROI_{lesion} (SI_{lesion}) in these three layers was measured, then the average value was calculated as the SI_{lesion} of the patient. An identical method was used to delineate another ROI on the same layer of normal intestinal wall ($ROI_{normal,}$ about 1 mm^2) and calculate its average signal intensity (SI_{normal}). Image noise was defined as the standard deviation (SD) for image background from the same area ROI as that used for SI_{lesion}. The formulas for signal-to-noise ratio (SNR) and contrast-to-noise ratio (CNR) were as follows (8,27):

$$SNR = \frac{SI_{lesion}}{SD_{lesion}} \quad [1]$$

$$CNR = \frac{\left|SI_{lesion} - SI_{normal}\right|}{\sqrt{SD^2_{lesion} + SD^2_{normal}}} \quad [2]$$

The agreement of T staging based on MRI (mrT staging) and pathological T staging (PT staging)

The two readers used the T staging standard of RC in TNM of American Joint Committee on Cancer 8th edition staging system as a reference standard, and used ACS-T2WI, CS-T2WI, and PI-T2WI combined with other scanning sequences to perform mrT staging respectively. Then, the accuracy of T staging of the three SR T2WI sequences and the consistency between the readers' mrT staging and PT staging were compared according to postoperative pathology results.

Statistical analysis

All statistical analyses were performed using SPSS 26.0 (IBM Corp., Armonk, NY, USA) and GraphPad Prism 9.5.0 (GraphPad Software, San Diego, CA, USA). Shapiro-Wilk test was used to test for normality of continuous variables. Continuous variables were expressed as means and SDs or medians and quartiles depending on whether the data were normally distributed; categorical variables were expressed

Table 2 Clinical characteristics of the patients

Characteristics	Value
Age (years)	65.79±13.09
Sex	
Male	19 (65.5)
Female	10 (34.5)
CEA level (ng/mL)	
<5	17 (60.7)
≥5	11 (39.3)
CA199 level (U/mL)	
<37	23 (82.1)
≥37	5 (17.9)
Tumor location	
Upper	4 (13.8)
Middle	21 (72.4)
Lower	4 (13.8)
pT stage	
T1	1 (3.4)
T2	2 (6.9)
T3	24 (82.8)
T4	2 (6.9)

Continuous variables following the normal distribution are expressed as means ± standard deviations, categorical variables are expressed as numbers (percentages). One patient's tumor marker turned out to be missing. CEA, carcinoembryonic antigen; CA199, carbohydrate antigen 199; pT stage, pathological T stage.

as percentages. The Friedman M test was used for group differences in Likert scores; *post hoc* analysis for Friedman's test was used to assess differences between each two groups. Agreement of Likert scores between two readers, the readers' mrT staging, and PT staging, were assessed with two-way mixed model absolute agreement intraclass correlation coefficient (ICC, 0.00–0.20, poor agreement; 0.21–0.40, fair agreement; 0.41–0.60, moderate agreement; 0.61–0.80, good agreement; and 0.81–1.00, excellent agreement). The accuracy of T staging was compared by Chi-squared test or Fisher's exact test. For quantitative analysis of data, sharpness, SNR, and CNR, if the error variances satisfied normality, randomized complete block design was used, otherwise, Friedman's test was used. *Post hoc* analysis for Bonferroni test or Friedman's test was used to assess differences between the two groups. A P value <0.05 indicated statistical significance.

Results

Patient characteristics

A total of 29 patients were enrolled in the study, including 19 males (65.5%) and 10 females (34.5%), aged 3–86 years with an average age of 65.79±13.09 years. Detailed patient characteristics including T-staging results are shown in *Table 2*.

Qualitative image analysis

The results of Likert scores assessed by two radiologists are shown in *Table 3* and *Figure 2*. All scores in *Table 3* are the average of two readers. For the visibility of structures, the scores of ACS-T2WI [median score, 4, interquartile range (IQR, 4, 4)] were higher than those of CS-T2WI [median score, 4 (IQR, 3, 4)] and PI T2WI [median score, 3.5 (IQR, 3, 4)], P<0.001; for the tissue edges sharpness, the scores of ACS-T2WI [median score, 3.5 (IQR, 3.5, 4)] were higher than those of CS-T2WI [median score, 3 (IQR, 2.5, 3)] and PI T2WI [median score, 3 (IQR, 2.5, 3)], P<0.001; for the overall image quality, the scores of ACS-T2WI [median score, 3.5 (IQR, 3.5, 4)] were higher than those of CS-T2WI [median score, 3 (IQR, 2.5, 3)] and PI T2WI [median score, 3 (IQR, 3, 3.5)], P<0.001; for confidence in N staging, the scores of ACS-T2WI [median score, 4 (IQR, 3.5, 4)] were higher than those of CS-T2WI [median score, 3 (IQR, 3, 3.75)] and PI T2WI [median score, 3 (IQR, 2.5, 3.5)], P<0.001; for image artifacts, there was no statistically significant difference among the three groups (P=0.18). The scores of visibility of structures, tissue edges sharpness, image artifacts, and confidence in N staging had good interobserver agreement, with ICC values of 0.73 [95% confidence interval (CI): 0.58–0.83], 0.71 (95% CI: 0.49–0.83), 0.68 (95% CI: 0.51–0.80), and 0.70 (95% CI: 0.55–0.81), respectively. The overall image quality scores had excellent interobserver agreement, 0.84 (95% CI: 0.76–0.90).

Quantitative analysis

The statistical results of sharpness, SNR, and CNR are shown in *Table 4* and *Figure 3*. The image sharpness of ACS-T2WI (0.093±0.019) was obviously higher than that of

Table 3 Qualitative image quality evaluation results of ACS-T2WI, CS-T2WI, and PI-T2WI

Parameter assessed	ACS-T2WI	CS-T2WI	PI-T2WI	F	P value	ICC*
Visibility of structures	4 (4, 4)[bc]	4 (3, 4)[a]	3.5 (3, 4)[a]	15.92	<0.001	0.73 (0.58, 0.83)
Tissue edges sharpness	3.5 (3.5, 4)[bc]	3 (2.5, 3)[a]	3 (2.5, 3)[a]	49.17	<0.001	0.71 (0.49, 0.83)
Image artifacts	4 (3, 4)	4 (3, 4)	3.5 (3, 4)	3.40	0.18	0.68 (0.51, 0.80)
Overall image quality	3.5 (3.5, 4)[bc]	3 (2.5, 3)[a]	3 (3, 3.5)[a]	28.54	<0.001	0.84 (0.76, 0.90)
Confidence in N staging	4 (3.5, 4)[bc]	3 (3, 3.75)[a]	3 (2.5, 3.5)[a]	27.82	<0.001	0.70 (0.55, 0.81)

All scores in this table are the average of two readers. Unless otherwise specified, data are expressed as median (quartiles interval). P<0.05 was considered statistically significant. *, data in parentheses are 95% CIs. [a], Friedman test with *post hoc*. P<0.05 versus ACS-T2WI; [b], Friedman test with *post hoc*. P<0.05 versus CS-T2WI; [c], Friedman test with *post hoc*. P<0.05 versus PI-T2WI. ACS, artificial intelligence-assisted compressed sensing; CS, compressed sensing; PI, parallel imaging; T2WI, T2-weighted imaging; F, Chi-squared values; ICC, intraclass correlation coefficient; CI, confidence interval.

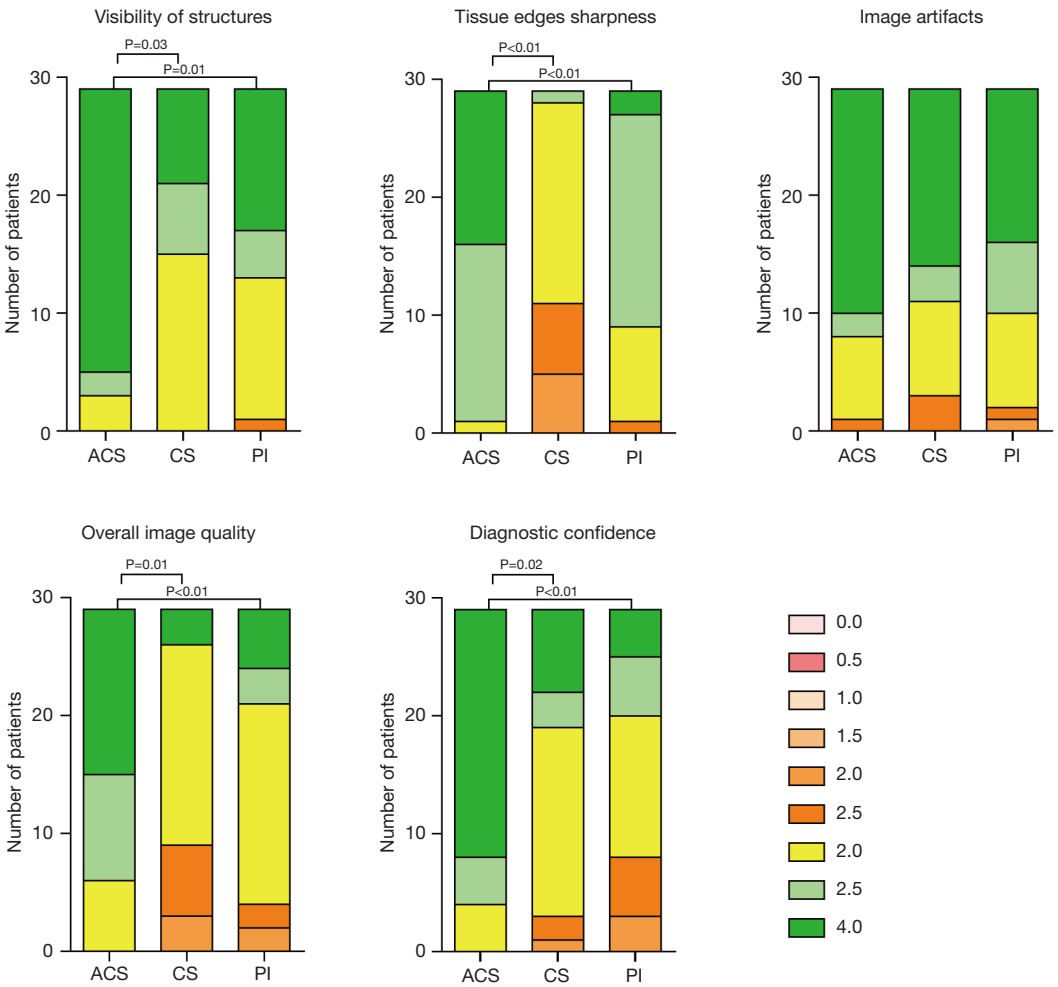

Figure 2 The stacked bar charts show the distribution of Likert scale scores used to assess qualitative image quality by sequence type. The score for each sequence is the average of the two readers. ACS, artificial intelligence-assisted compressed sensing (the Likert scale scores of ACS-T2WI); CS, compressed sensing (the Likert scale scores of CS-T2WI); PI, parallel imaging (the Likert scale scores of PI-T2WI); T2WI, T2-weighted imaging;

Table 4 Quantitative evaluation results of ACS-T2WI, CS-T2WI and PI-T2WI

Parameter	ACS-T2WI	CS-T2WI	PI-T2WI	F	P value
Sharpness	0.093±0.019[bc]	0.061±0.007[a]	0.067±0.008[a]	151.57	<0.001
SNR	13.71 (12.27,15.51)[b]	17.33±5.28[ac]	14.91±3.66[b]	3.54	0.004
CNR	5.57±3.04	5.18±2.89	5.39±3.61	0.87	0.425

Values are expressed as mean ± standard deviation or median (quartiles interval) according to the normal distribution of the data. P<0.05 was considered statistically significant. [a], *post hoc* Bonferroni test P<0.05 versus ACS-T2WI; [b], *post hoc* Bonferroni test P<0.05 versus CS-T2WI; [c], *post hoc* Bonferroni test P<0.05 versus PI-T2WI. ACS, artificial intelligence-assisted compressed sensing; CS, compressed sensing; PI, parallel imaging; T2WI, T2-weighted imaging; F, Chi-squared values; SNR, signal-to-noise ratio; CNR, contrast-to-noise ratio.

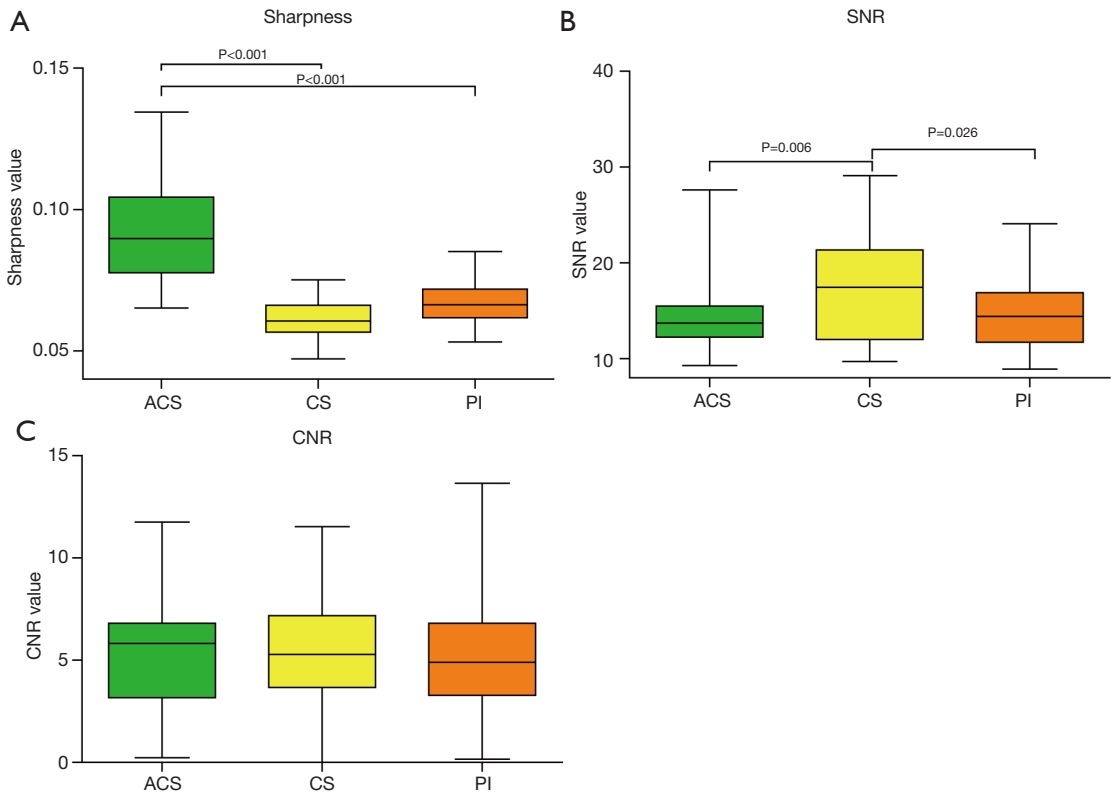

Figure 3 Box-and-Whisker plots for quantitative parameters. (A) Sharpness of ACS-T2WI, CS-T2WI, and PI-T2WI; (B) SNR of ACS-T2WI, CS-T2WI, and PI-T2WI; (C) CNR of ACS-T2WI, CS-T2WI, and PI-T2WI. The three horizontal lines in the Box-and-Whisker plots represent the 25th percentile, the 50th percentile, and the 75th percentile from top to bottom. T2WI, T2-weighted imaging; ACS, artificial intelligence-assisted compressed sensing; CS, compressed sensing; PI, parallel imaging; SNR, signal-to-noise ratio; CNR, contrast-to-noise ratio.

CS-T2WI (0.061±0.007) and PI-T2WI (0.067±0.008), and there was no statistical difference between CS-T2WI and PI-T2WI. The SNR of CS-T2WI (17.33±5.28) was higher than ACS-T2WI and PI-T2WI [median score, 13.71 (IQR, 12.27, 15.51), 14.91±3.66, respectively; P=0.004]. The CNR of ACS-T2WI (5.57±3.04) was slightly higher than that of CS-T2WI (5.18±2.89) and PI-T2WI (5.39±3.61), but the difference was not statistically significant (P=0.425).

mrT staging and pathological T stage agreement

Tables 5,6 show the results of comparison between every

Table 5 Reader 1's contingency table of PT staging and mrT staging

PT staging	ACS-T staging				CS-T staging				PI-T staging			
	T1	T2	T3	T4	T1	T2	T3	T4	T1	T2	T3	T4
T1	1	0	0	0	1	0	0	0	1	0	0	0
T2	0	2	0	0	0	1	1	0	0	1	1	0
T3	0	1	21	2	0	2	19	3	0	3	18	3
T4	0	0	0	2	0	0	0	2	0	0	0	2

PT staging, pathological T staging; mrT staging, T staging based on MRI; ACS-T staging, mrT staging based on the ACS-T2WI; CS-T staging, mrT staging based on the CS-T2WI; PI-T staging, mrT staging based on the PI-T2WI; ACS, artificial intelligence assisted compressed sensing; CS, compressed sensing; PI, parallel imaging; T2WI, T2-weighted imaging.

Table 6 Reader 2's contingency table of PT staging and mrT staging

PT staging	ACS-T staging				CS-T staging				PI-T staging			
	T1	T2	T3	T4	T1	T2	T3	T4	T1	T2	T3	T4
T1	1	0	0	0	1	0	0	0	1	0	0	0
T2	0	1	1	0	0	0	2	0	0	0	2	0
T3	0	1	23	0	0	2	22	0	0	3	20	1
T4	0	0	1	1	0	0	1	1	0	0	1	1

PT staging, pathological T staging; mrT staging, T staging based on MRI; ACS-T staging, mrT staging based on the ACS-T2WI; CS-T staging, mrT staging based on the CS-T2WI; PI-T staging, mrT staging based on the PI-T2WI; T2WI, T2-weighted imaging; ACS, artificial intelligence assisted compressed sensing; CS, compressed sensing; PI, parallel imaging.

reader's mrT staging and PT staging of each sequence. For reader 1, the agreement between the T staging of the ACS-T2WI, CS-T2WI, and PI-T2WI and the PT staging were 0.85, 0.71, and 0.67, respectively. For reader 2, these values were 0.80, 0.63, and 0.59, respectively. Readers had a higher diagnostic accuracy of ACS-T2WI (89.66%) than they did of CS-T2WI (79.31%) and PI-T2WI (75.86%), but the difference was not statistically significant (P=0.47).

Discussion

In this study, SR T2WI rectal images based on ACS were evaluated by comparing them with images based on CS and PI. The results showed that ACS-T2WI performed better than CS-T2WI and PI-T2WI in qualitative image assessment such as structure visibility, edge sharpness, overall image quality, and confidence in N staging (inter-reader agreement was good or excellent). ACS-T2WI showed better sharpness than CS-T2WI and PI-T2WI in quantitative image quality comparison. The SNR of ACS-T2WI was slightly lower than that of CS-T2WI, but comparable to that of PI-T2WI. ACS-T2WI mrT staging is more consistent with PT staging than CS-T2WI and PI-T2WI. Therefore, we conclude that SR T2WI based on ACS is helpful for T and N staging of RC patients with the reasonable scanning time, which has potential to improve the performance of RC diagnosis and has a good application prospect in RC MRI.

Balancing the spatial resolution, contrast resolution, and temporal resolution of MRI has always been a major difficulty. The matrix in MRI is closely related to the image resolution. The larger the matrix is, the smaller the pixels are, and the clearer the image details are. If only increasing the image matrix, the scan time will multiply, which cannot be tolerated by many patients. Previous studies have shown that MRI technology based on DL reconstruction can shorten the scan time while maintaining image quality, and can also provide SR images for some diseases when required (28,29). At present, ACS is often used to shorten the examination time of various parts of MRI, avoid the

repeated examination caused by patient intolerance, and reduce the examination cost, so as to increase the flow of patients (7,25). However, for some diseases, SR images need to be acquired for accurate diagnosis and quantitative analysis (30). Chaudhari *et al.* (31) found that MRI images of osteoarthritis based on DL were superior to conventional SR images based on interpolation techniques in image sharpness, image blur measurement, and cartilage detection, and the image quality could be improved without bias to quantitative biomarkers. When Zhou *et al.* (32) studied SR brain tumor MRI based on DL, they found that the SR T2-fluid attenuated inversion recovery (FLAIR) images had an improved Dice coefficient compared to the original low-resolution T2-FLAIR images; MRI-based brain tumor SR generative adversarial network modified from enhanced SR generative adversarial network architecture had great potential in early detection and accurate evaluation of brain tumor recurrence and prognosis. Almansour *et al.* (33) combined DL-based SR with a PF reconstruction technique for abdominal gradient echo sequence, which can shorten the breath-holding time and improve the image clarity and lesion significance.

For RC patients, previous studies have shown that T2WI with smaller voxels has advantages in lesion detection, can reduce the occurrence of partial volume effect, and clearly show the edge of the lesion and the depth of extramural invasion, which is crucial for the T and N staging of RC (27,34). Hou *et al.* (35) used three-dimensional (3D) SR images based on DL for radiomics analysis for the first time and found that the SR radiomics model showed a more favorable ability to help clinicians evaluate the invasion depth of RC before surgery. In this study, we observed a slightly lower SNR for ACS-T2WI compared to CS-T2WI, likely due to the substantial increase in the image matrix size from 512×512 to 704×704, which directly enhances spatial resolution. This improvement in resolution is a key objective of our approach, demonstrating the effectiveness of ACS technology in achieving higher resolution images without increasing scan time. So, ACS-T2WI can improve the success rate of examination with the same scanning time (168 s). It can use a higher matrix to increase the image resolution, and the contrast between the lesion edge and the normal bowel wall is sharper, which is helpful to accurately distinguish the structures (*Figure 4*) of the rectum and T stage. The T staging consistency of ACS-T2WI was higher than that of CS-T2WI and PI-T2WI, and the T staging of ACS-T2WI had the potential to be better than the other two sequences, but the results were not statistically significant. The staging of lymph node metastasis is crucial for the selection of treatment methods for RC. A total of 29 patients with RC who met the inclusion and exclusion criteria were collected. The exclusion of patients without lymph node metastasis would have reduced the number of eligible patients even further if the results of lymph node metastasis evaluation in the three sequences were matched with the histopathological results one-to-one, and there is concern that the statistical results may have been due to substantial chance. Therefore, the diagnostic confidence of N staging in the qualitative evaluation was specifically designed. The results showed that the diagnostic confidence of N staging on ACS-T2WI was higher than that on CS-T2WI and PI-T2WI (*Figure 5*). The two readers' image quality assessment indicated that ACS-T2WI can provide more evidence of lymph node metastasis than CS-T2WI and PI-T2WI, thereby improving diagnostic confidence. However, this increased confidence was not matched with histopathology, so the accuracy of ACS-T2WI remains uncertain. At present, even experienced radiologists are not accurate in the diagnosis of lymph node metastasis in RC (36). The potential for ACS-T2WI to provide improved diagnosis of lymph node metastasis less than 5 mm will be explored in future studies.

This study has some limitations. First, it was a single-center study. Due to the need for quantitative data measurement, only a relatively small number of patients with rectal adenocarcinoma were included in this study, and further prospective studies with a large number of patients in multi-centers are needed. Second, other acceleration factors and combinations of other matrix sizes were not compared, given patient tolerance and acquisition time.

Conclusions

By using ACS to increase the resolution through a larger matrix size, higher quality images can be obtained within the same scanning time as traditional acceleration techniques. This technique is superior to CS-T2WI and PI-T2WI in image sharpness, lesion structure visibility, and N staging of RC. It has a good application prospect in clinical MRI scanning of RC.

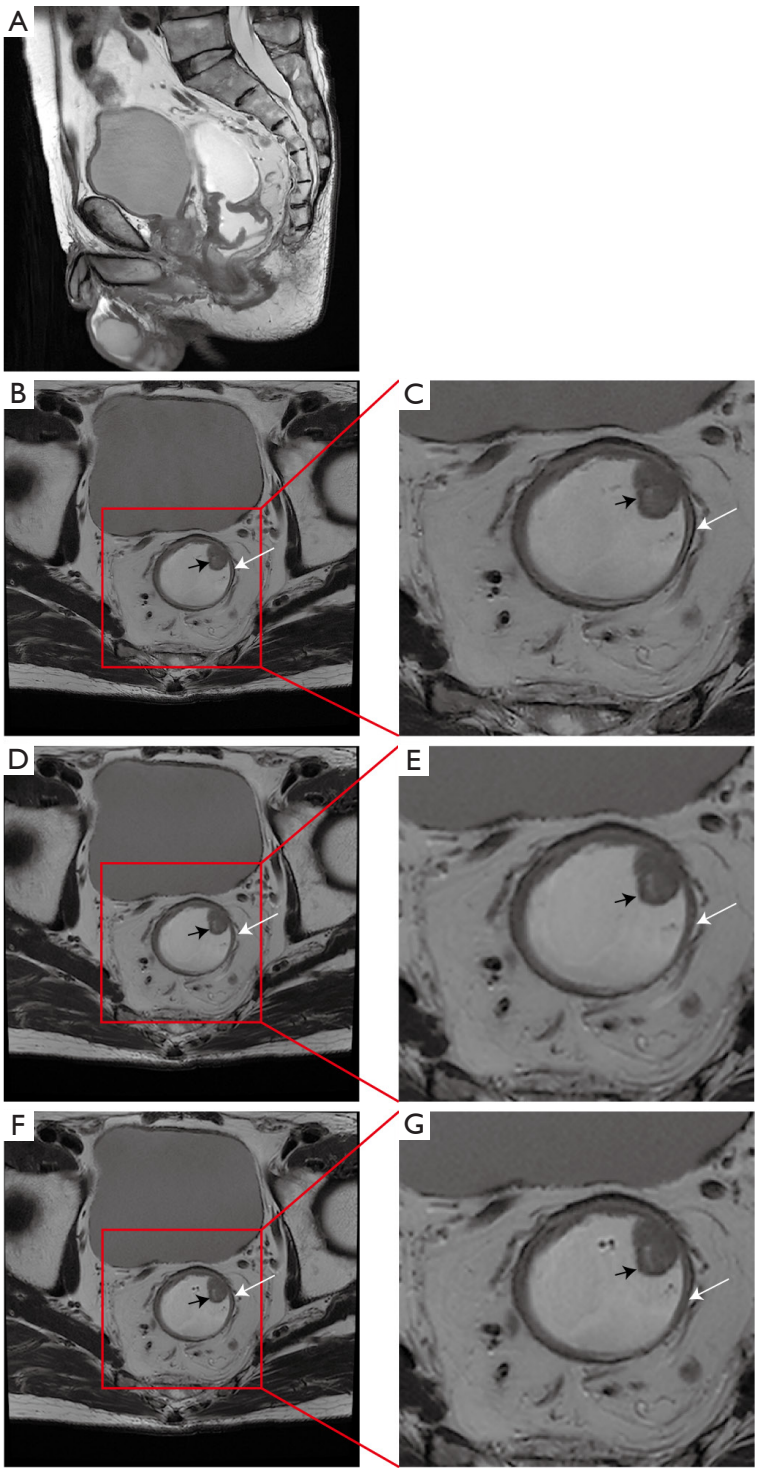

Figure 4 MRI of a 68-year-old male patient with pathologically diagnosed T3 rectal cancer. (A) The sagittal image; (B,C) the images of ACS-T2WI; (D,E) the images of CS-T2WI; (F,G) the images of PI-T2WI. Where (B,D,F) are the original images and (C,E,G) are the magnified images, the magnification is 2.2. The black arrows represent rectal cancer lesions, the white arrows represent the rectal wall and the selected part in the red box is the enlarged part. The visualization of intestinal wall on ACS-T2WI images are better than that on CS-T2WI and PI-T2WI images. MRI, magnetic resonance imaging; T2WI, T2-weighted imaging; ACS, artificial intelligence-assisted compressed sensing; CS, compressed sensing; PI, parallel imaging.

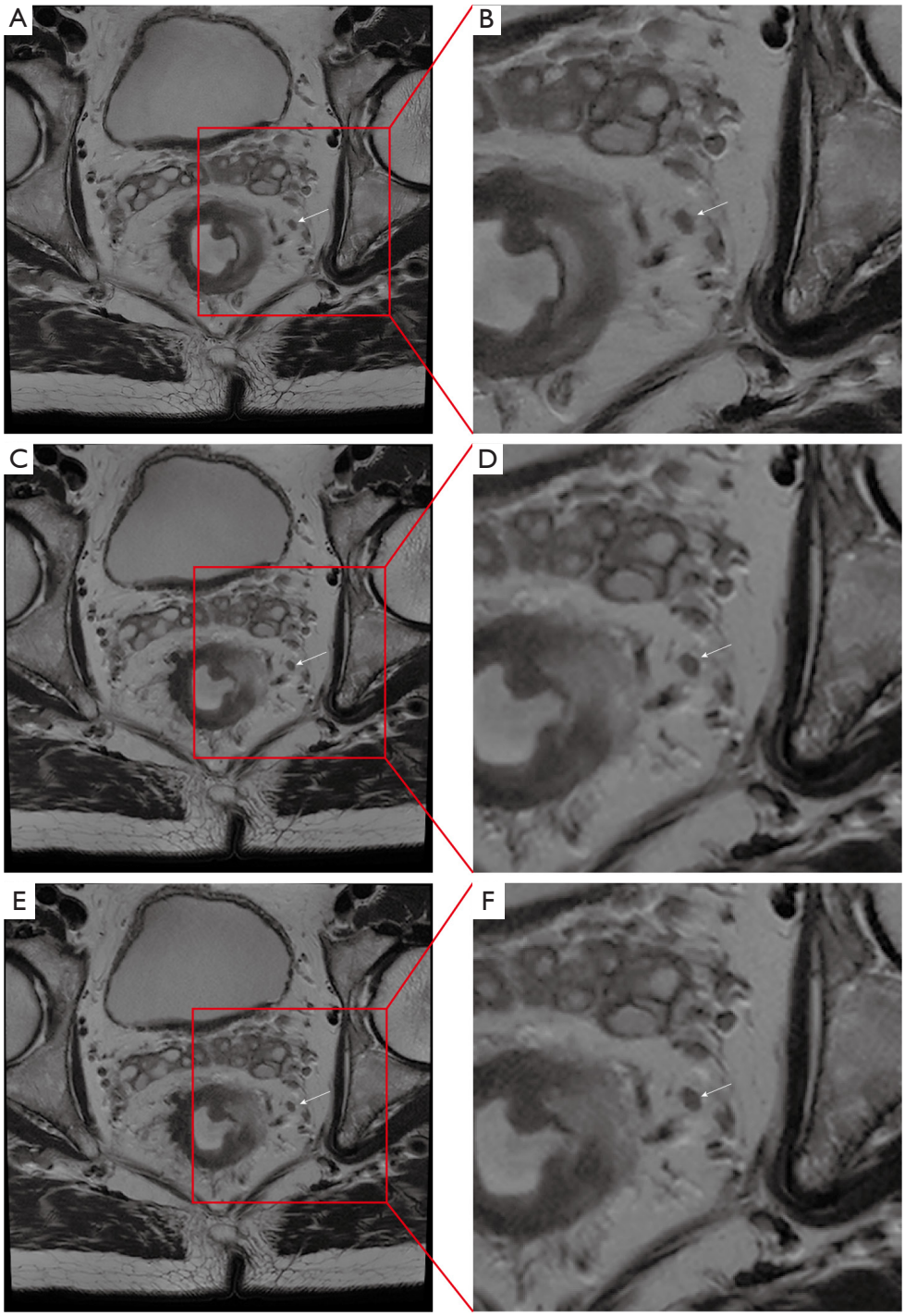

Figure 5 MRI of another 68-year-old male patient with pathologically diagnosed T3 rectal cancer. (A,B) The picture of ACS-T2WI; (C,D) the picture of CS-T2WI; (E,F) the picture of PI-T2WI. Where (A,C,E) are the original images and (B,D,F) are the magnified images, the magnification is 2. White arrows point to lymph node, the selected part in the red box is the enlarged part. On the ACS-T2WI images, the margins of lymph nodes were irregular, suggesting a higher suspicion of lymph node metastasis of rectal cancer. However, on the CS-T2WI and PI-T2WI images, the blurred margins made it difficult to assess lymph node metastasis. MRI, magnetic resonance imaging; T2WI, T2-weighted imaging; ACS, artificial intelligence assisted compressed sensing; CS, compressed sensing; PI, parallel imaging.

Acknowledgments

Thanks to the Department of Radiology, The First Affiliated Hospital of Shandong First Medical University for supporting this study.

Footnote

Reporting Checklist: The authors have completed the GRRAS reporting checklist. Available at https://qims.amegroups.com/article/view/10.21037/qims-24-1317/rc

Funding: This work was supported by Shandong First Medical University (Shandong Academy of Medical Sciences) Youth Science Foundation Cultivation Grant Program (No. 202201-080), Technology Development Plan of Shandong Province (No. 2014GSF118091), and the Shandong Medical and Health Science and Technology Development Plan (No. 2017WS715).

Conflicts of Interest: All authors have completed the ICMJE uniform disclosure form (available at https://qims.amegroups.com/article/view/10.21037/qims-24-1317/coif). The authors have no conflicts of interest to declare.

Ethical Statement: The authors are accountable for all aspects of the work in ensuring that questions related to the accuracy or integrity of any part of the work are appropriately investigated and resolved. This study was conducted in accordance with the Declaration of Helsinki (as revised in 2013). The prospective study from June 2023 to January 2024 was approved by Medical Ethics Committee of The First Affiliated Hospital of Shandong First Medical University (No. YXLL-KY-073), and all participants signed written informed consent.

References

1. Sung H, Ferlay J, Siegel RL, Laversanne M, Soerjomataram I, Jemal A, Bray F. Global Cancer Statistics 2020: GLOBOCAN Estimates of Incidence and Mortality Worldwide for 36 Cancers in 185 Countries. CA Cancer J Clin 2021;71:209-49.
2. Dekker E, Tanis PJ, Vleugels JLA, Kasi PM, Wallace MB. Colorectal cancer. Lancet 2019;394:1467-80.
3. Keller DS, Berho M, Perez RO, Wexner SD, Chand M. The multidisciplinary management of rectal cancer. Nat Rev Gastroenterol Hepatol 2020;17:414-29.
4. Chen F, Zhang S, Ma X, Chen Y, Wang Z, Zhu Y, Bai C, Fu C, Grimm R, Shao C, Lu J, Shen F, Chen L. Prediction of tumor budding in patients with rectal adenocarcinoma using b-value threshold map. Eur Radiol 2023;33:1353-63.
5. Horvat N, Carlos Tavares Rocha C, Clemente Oliveira B, Petkovska I, Gollub MJ. MRI of Rectal Cancer: Tumor Staging, Imaging Techniques, and Management. Radiographics 2019;39:367-87.
6. Ma L, Lian S, Liu H, Meng T, Zeng W, Zhong R, Zhong L, Xie C. Diagnostic performance of synthetic magnetic resonance imaging in the prognostic evaluation of rectal cancer. Quant Imaging Med Surg 2022;12:3580-91.
7. Ni M, He M, Yang Y, Wen X, Zhao Y, Gao L, Yan R, Xu J, Zhang Y, Chen W, Jiang C, Li Y, Zhao Q, Wu P, Li C, Qu J, Yuan H. Application research of AI-assisted compressed sensing technology in MRI scanning of the knee joint: 3D-MRI perspective. Eur Radiol 2024;34:3046-58.
8. Yang F, Pan X, Zhu K, Xiao Y, Yue X, Peng P, Zhang X, Huang J, Chen J, Yuan Y, Sun J. Accelerated 3D high-resolution T2-weighted breast MRI with deep learning constrained compressed sensing, comparison with conventional T2-weighted sequence on 3.0 T. Eur J Radiol 2022;156:110562.
9. Montalt-Tordera J, Muthurangu V, Hauptmann A, Steeden JA. Machine learning in Magnetic Resonance Imaging: Image reconstruction. Phys Med 2021;83:79-87.
10. Tian C, Ma X, Lu H, Wang Q, Shao C, Yuan Y, Shen F. Deep learning models for preoperative T-stage assessment in rectal cancer using MRI: exploring the impact of rectal filling. Front Med (Lausanne) 2023;10:1326324.
11. Sluckin TC, Hekhuis M, Kol SQ, Nederend J, Horsthuis K, Beets-Tan RGH, Beets GL, Burger JWA, Tuynman JB, Rutten HJT, Kusters M, Benson S. A Deep Learning Framework with Explainability for the Prediction of

Lateral Locoregional Recurrences in Rectal Cancer Patients with Suspicious Lateral Lymph Nodes. Diagnostics (Basel) 2023.
12. Matsumoto S, Tsuboyama T, Onishi H, Fukui H, Honda T, Wakayama T, Wang X, Matsui T, Nakamoto A, Ota T, Kiso K, Osawa K, Tomiyama N. Ultra-High-Resolution T2-Weighted PROPELLER MRI of the Rectum With Deep Learning Reconstruction: Assessment of Image Quality and Diagnostic Performance. Invest Radiol 2024;59:479-88.
13. Liu Y, Shi J, Liu W, Tang Y, Shu X, Wang R, Chen Y, Shi X, Jin J, Li D. A deep neural network predictor to predict the sensitivity of neoadjuvant chemoradiotherapy in locally advanced rectal cancer. Cancer Lett 2024;589:216641.
14. Li J, Song Y, Wu Y, Liang L, Li G, Bai S. Clinical evaluation on automatic segmentation results of convolutional neural networks in rectal cancer radiotherapy. Front Oncol 2023;13:1158315.
15. Jin Y, Yin H, Zhang H, Wang Y, Liu S, Yang L, Song B. Predicting tumor deposits in rectal cancer: a combined deep learning model using T2-MR imaging and clinical features. Insights Imaging 2023;14:221.
16. Geldof F, Pruijssers CWA, Jong LS, Veluponnar D, Ruers TJM, Dashtbozorg B. Tumor Segmentation in Colorectal Ultrasound Images Using an Ensemble Transfer Learning Model: Towards Intra-Operative Margin Assessment. Diagnostics (Basel) 2023.
17. Wong C, Fu Y, Li M, Mu S, Chu X, Fu J, Lin C, Zhang H. MRI-Based Artificial Intelligence in Rectal Cancer. J Magn Reson Imaging 2023;57:45-56.
18. Zhao Q, Xu J, Yang YX, Yu D, Zhao Y, Wang Q, Yuan H. AI-assisted accelerated MRI of the ankle: clinical practice assessment. Eur Radiol Exp 2023;7:62.
19. Almansour H, Herrmann J, Gassenmaier S, Afat S, Jacoby J, Koerzdoerfer G, Nickel D, Mostapha M, Nadar M, Othman AE. Deep Learning Reconstruction for Accelerated Spine MRI: Prospective Analysis of Interchangeability. Radiology 2023;306:e212922.
20. Chang PD, Chow DS. Revolutionizing Shoulder MRI: Accelerated Imaging with Deep Learning Reconstruction. Radiology 2024;310:e233301.
21. Tanabe M, Higashi M, Yonezawa T, Yamaguchi T, Iida E, Furukawa M, Okada M, Shinoda K, Ito K. Feasibility of high-resolution magnetic resonance imaging of the liver using deep learning reconstruction based on the deep learning denoising technique. Magn Reson Imaging 2021;80:121-6.
22. Yan X, Ran L, Zou L, Luo Y, Yang Z, Zhang S, Zhang S, Xu J, Huang L, Xia L. Dark blood T2-weighted imaging of the human heart with AI-assisted compressed sensing: a patient cohort study. Quant Imaging Med Surg 2023;13:1699-710.
23. Bischoff LM, Peeters JM, Weinhold L, Krausewitz P, Ellinger J, Katemann C, Isaak A, Weber OM, Kuetting D, Attenberger U, Pieper CC, Sprinkart AM, Luetkens JA. Deep Learning Super-Resolution Reconstruction for Fast and Motion-Robust T2-weighted Prostate MRI. Radiology 2023;308:e230427.
24. Xie Y, Tao H, Li X, Hu Y, Liu C, Zhou B, Cai J, Nickel D, Fu C, Xiong B, Chen S. Prospective Comparison of Standard and Deep Learning-reconstructed Turbo Spin-Echo MRI of the Shoulder. Radiology 2024;310:e231405.
25. Yasaka K, Tanishima T, Ohtake Y, Tajima T, Akai H, Ohtomo K, Abe O, Kiryu S. Deep learning reconstruction for 1.5 T cervical spine MRI: effect on interobserver agreement in the evaluation of degenerative changes. Eur Radiol 2022;32:6118-25.
26. Li X, editor. Blind image quality assessment. Proceedings. International Conference on Image Processing; IEEE 2002. doi: 10.1109/ICIP.2002.1038057.
27. Zhou M, Gong T, Chen M, Wang Y. High-resolution integrated dynamic shimming diffusion-weighted imaging (DWI) in the assessment of rectal cancer. Eur Radiol 2023;33:5769-78.
28. Lin DJ, Walter SS, Fritz J. Artificial Intelligence-Driven Ultra-Fast Superresolution MRI: 10-Fold Accelerated Musculoskeletal Turbo Spin Echo MRI Within Reach. Invest Radiol 2023;58:28-42.
29. Qiu D, Cheng Y, Wang X. Medical image super-resolution reconstruction algorithms based on deep learning: A survey. Comput Methods Programs Biomed 2023;238:107590.
30. Yang G, Zhang L, Liu A, Fu X, Chen X, Wang R. MGDUN: An interpretable network for multi-contrast MRI image super-resolution reconstruction. Comput Biol Med 2023;167:107605.
31. Chaudhari AS, Stevens KJ, Wood JP, Chakraborty AK, Gibbons EK, Fang Z, Desai AD, Lee JH, Gold GE, Hargreaves BA. Utility of deep learning super-resolution in the context of osteoarthritis MRI biomarkers. J Magn Reson Imaging 2020;51:768-79.
32. Zhou Z, Ma A, Feng Q, Wang R, Cheng L, Chen X, Yang X, Liao K, Miao Y, Qiu Y. Super-resolution of brain tumor MRI images based on deep learning. J Appl Clin Med Phys

2022;23:e13758.
33. Almansour H, Herrmann J, Gassenmaier S, Lingg A, Nickel MD, Kannengiesser S, Arberet S, Othman AE, Afat S. Combined Deep Learning-based Super-Resolution and Partial Fourier Reconstruction for Gradient Echo Sequences in Abdominal MRI at 3 Tesla: Shortening Breath-Hold Time and Improving Image Sharpness and Lesion Conspicuity. Acad Radiol 2023;30:863-72.
34. Yang YS, Qiu YJ, Zheng GH, Gong HP, Ge YQ, Zhang YF, Feng F, Wang YT. High resolution MRI-based radiomic nomogram in predicting perineural invasion in rectal cancer. Cancer Imaging 2021;21:40.
35. Hou M, Zhou L, Sun J. Deep-learning-based 3D super-resolution MRI radiomics model: superior predictive performance in preoperative T-staging of rectal cancer. Eur Radiol 2023;33:1-10.
36. Xian MF, Zheng X, Xu JB, Li X, Chen LD, Wang W. Prediction of lymph node metastasis in rectal cancer: comparison between shear-wave elastography based ultrasomics and MRI. Diagn Interv Radiol 2021;27:424-31.

Cite this article as: Zheng G, Fu J, Wang Z, Li W, Li A, Yu D. AI-assisted compressed sensing MRI improves imaging quality in rectal cancer: a comparative study with conventional acceleration techniques. Quant Imaging Med Surg 2025;15(3):2547-2560. doi: 10.21037/qims-24-1317